EXPERIMENTAL MONITORING OF VIBRATIONS AND THE PROBLEM OF AMPLITUDE QUANTIFICATION

Alexandra P. Schneider*
Benoit Paoletti
Xavier Ottavy
Christoph Brandstetter
Univ. de Lyon, Ecole Centrale de Lyon,
CNRS, LMFA, UMR 5509, F-69134, ECULLY,
France

ABSTRACT

Experimental monitoring of blade vibration in turbomachinery is typically based on blade-mounted strain gauges. Their signals are used to derive vibration amplitudes which are compared to previously determined modal scope limits, including a safety factor. According to industrial guidelines, this factor is chosen conservatively to ensure safe operation of the machine.

For the experimental campaign with the open test case fan ECL5, which is representative for modern lightweight UHBR architectures, it is planned to conduct measurements close to the stability limit. These investigations require a close approach to the limit and hence demand for accurate quantification of vibration amplitudes to ensure secure operation without exhaustive safety margins. It is required that the surveillance is possible in real time and not only in post-processing.

Historically, short-time Fourier transformations of vibration sensors are used, but the complex nature of coupled phenomena near the stability limit has an influence on the amplitude accuracy, depending on evaluation parameters. This was demonstrated in a previous study using fast response wall pressure transducers. The present study investigates the influence on blade vibration data of a modern composite material transonic fan. Different methods are compared, sensitivity to evaluation parameters is analyzed and guidelines are given for fast and robust surveillance of critical vibration modes.

NOMENCLATURE

a	correction parameter
b	ratio of spectral amplitude and real amplitude
d	viscous damping ratio
DS	Design Speed
ECL	Ecole Centrale de Lyon
EO	Engine Order
f_{mode1}	eigenfrequency of mode 1 [Hz]
f_s	sampling frequency [Hz]
f_{res}	frequency resolution [Hz]
Δf	bin width [Hz]
F	Force
FFT, FT	(Fast) Fourier Transformation
$\mathscr{F}(x(t))$	Fourier Transform of signal $x(t)$
$H(\omega)$	transfer function
k	stiffness
$\dot{m}$	massflow
m	mass
N	number of samples per FT-window
NSV	Non Synchronous Vibrations
RMS	Root Mean Square
p	pressure
P	total power
PIV	Particle Image Velocimetry
PS	Part Speed
PSD	Power Spectral Density
S_{xx}	power spectral density
ST	Short Time
t	time
Δt	FT window size [s]
T	measurement period
$w[n]$	window function
X_k	Discrete Fourier Transform of signal $x[n]$
$\hat{x}$	amplitude
Π_t	Total Pressure Ratio
ζ	damping ratio
Ω_r^S	angular frequency of the rotor [rad/s]
ω_v^R	vibration frequency [rad/s]
ω_0	eigenfrequency of the SDOF model [rad/s]

INTRODUCTION

Within the European project CATANA the open test case fan ECL5 (see [1,2] for details) will be used to perform experiments near the stability limit to investigate aeroelastic phenomena like flutter or non-synchronous vibration (NSV). In modern fan architectures, these phenomena lead to rapidly rising blade vibration and blade failure. Thus, operation close to those regions is extremely safety critical.
Established test procedures for this kind of measurements are based on industrial guidelines resulting in conservative security limits, which ensure the structural integrity of the machine

*corresponding author

during operation and account for inaccuracies in measurement and evaluation methods. To allow stabilized measurements like Particle Image Velocimetry (PIV) close to the stability limit, established procedures need to be revised as extensive safety margins currently prevent anticipated campaigns.

Experimental surveillance of blade vibration is essential to avoid blade failure during operation. Since the early 1950 years, this is commonly done by the use of blade-mounted strain gauges [3, 4, 5]. To measure rotor blade vibration, signals are transferred via slip rings or telemetry to the stationary frame of reference. Based on spectral analysis methods these signals can be used for real-time surveillance of vibrational frequencies and related amplitudes, which can be compared to previously defined scope limits.

For ECL5 experiments, it is necessary to minimize the safety factor typically considered during calculation of scope limits. At the same time it has to be ensured that calculated spectral amplitudes are independent from chosen method parameters to allow for correct assessment of blade stresses and safe operation.

In an experimental investigation of the fan used for the present study, Brandstetter et al. [6] observed that spectral pressure amplitude decreases up to 50% if the short-time fast Fourier transform (ST-FFT) window size is increased from 5 to 25 rotor revolutions when approaching the stability limit. This behaviour was associated to non-harmonic disturbances and subsequent influence on spectral analysis methods. The results presented in [6] only concerned physical interpretation, but in the case of vibration surveillance by means of strain gauges such a dependency can result in a safety-critical underestimation of vibration levels.

The shortcomings of Fourier transform (FT) for fluctuating signals with unsteady frequency content are well known, and literature proposes the use of power spectral density (PSD) estimations, as results are more robust towards evaluation parameters such as window size (and hence frequency resolution) [7]. However, resulting spectra are given in the unit of $\hat{x}^2/\mathrm{Hz}$, which cannot be directly compared to material scope limits.
As will be shown in this study, the advantage of PSD compared to FT disappears, if spectra are converted into scope limit amplitudes and a robust spectral surveillance method for turbomachinery vibrations must be developed. It will be shown, that configuration specific amplitude correction approaches can be useful and generalized (calibrated) for specific architectures.

The presented study provides an investigation of spectral analysis methods, based on real-engine test data and artificial signals to investigate sensitivity.

The study is structured as follows:

· brief introduction of experimental setup and test procedure
· summary of mathematical description of spectral analysis methods
· review of the influence of frequency resolution on FT and PSD and formulation of problem
· derivation of a correction approach
· presentation of corrected results and discussion

TEST FACILITY ECL-B3

The test facility ECL-B3 presented in Fig. 1 was designed and built in cooperation between Ecole Centrale de Lyon (ECL) and Safran Aircraft Engines (Safran AE) through the ANR- EQUIPEX program. It is used for investigations of fan architectures representative of modern UHBR stages at scales around 1:4.

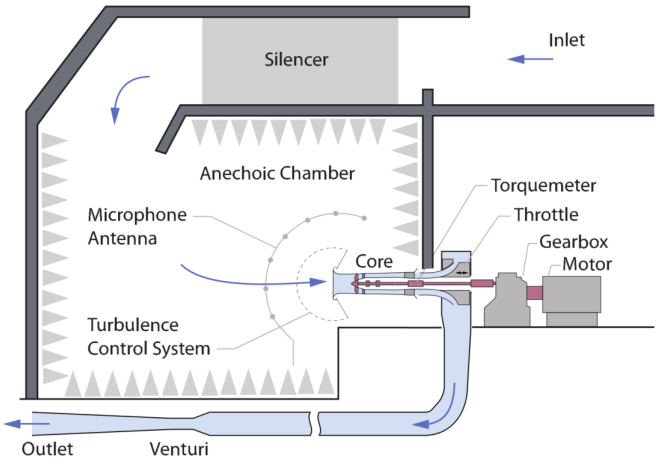

Fig. 1: **SCHEMATIC VIEW OF ECL-B3 TEST FACILITY**

The measurements considered in this study have been performed within the ENOVAL project. The investigated stage consists of a composite, low speed transonic fan and outlet guide vanes (OGV), designed by Safran AE. It is placed in an anechoic chamber and operated in an open cycle. Air is sucked in from the roof, passes the core section i.e the fan stage and the axisymmetric coned shaped throttle and exits through an exhaust system to atmosphere.

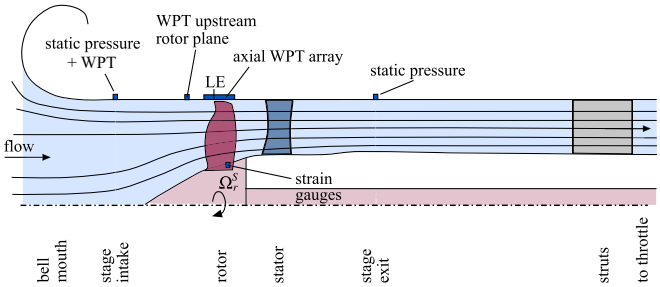

Fig. 2: **SCHEMATIC VIEW OF THE MACHINE CORE AND PROBE POSITIONS**

The machine core, schematically shown in Fig. 2, allows time-efficient and flexible change of test configurations. It is instrumented with pressure and temperature sensors, distributed in various meridian positions on the hub and casing as well as in rakes, to allow performance quantification.

Besides flush-mounted static pressure probes, miniature high frequency response wall pressure transducers (WPT) and microphones are placed in various axial and circumferential positions to observe unsteady aerodynamics in the machine. The measurement of structural vibrations, analyzed

within this study, is implemented through blade-mounted strain gauges on the rotor, transferred via telemetry.

Details on facility and instrumentation are given in [8].

Test procedure

The ENOVAL test campaign consisted of two procedures: the fan mapping measurements, with full traversals of the stage exit plane at stable operating conditions, and the operability measurements during which the machine was transiently throttled towards/ beyond the stability limit.
For the present study, only operating points close to the stability limit and transient throttling manoeuvres are of interest, but the developed methodology can be applied to all other operating points as well.

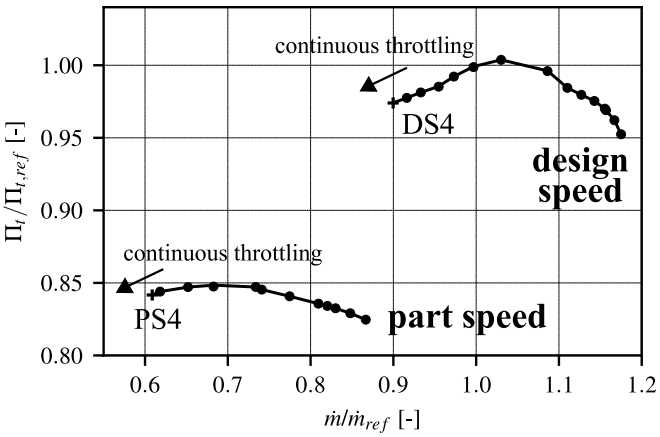

Fig. 3: **FAN PERFORMANCE MAP AND INVESTIGATED OPERATING POINTS**

Fig. 3 illustrates the pressure ratio as a function of massflow (normalized with the massflow of the peak pressure operating point at design speed $\dot{m}_{ref}$) for the speedlines and operating points under investigation.

SPECTRAL ANALYSIS METHODOLOGY

This section presents a short review of the spectral analysis methods, which are used within this study to identify the frequency content of a signal and corresponding amplitudes. As will be shown in the following sections, the well established procedures are not robust to specific parameters concerning the derived amplitudes.

For a continuous signal

$$x = f(t) \tag{1}$$

the Fourier transform (FT) is defined as

$$\mathscr{F}(f) = \int_{-\infty}^{\infty} x(t) \cdot e^{-i2\pi ft} dt \tag{2}$$

and gives information about the amplitude for each (positive and negative) frequency. Accordingly, the FT of a discrete time series with N samples

$$x[n] = x_0, x_1, \ldots, x_{N-1} \tag{3}$$

is given by

$$X_k = \sum_{n=0}^{N-1} x_n \cdot e^{-\frac{i2\pi}{N} kn} \tag{4}$$

The total power of a signal $x(t)$ can be calculated using

$$P = \lim_{T\to\infty} \frac{1}{T} \int_{-T/2}^{T/2} |x(t)|^2 dt \tag{5}$$

If Parseval's Theorem

$$\int_{-\infty}^{\infty} |x(t)|^2 dt = \int_{-\infty}^{\infty} |x(2\pi f)|^2 df \tag{6}$$

is applied, Eq. 5 can be expressed as a function of $\mathscr{F}(f)$

$$P = \lim_{T\to\infty} \frac{1}{T} \cdot \int_{-\infty}^{\infty} |x(f)|^2 df \tag{7}$$

The integrand of this equation is defined as the power spectral density

$$S_{xx}(f) = \lim_{T\to\infty} \frac{1}{T} |x(f)|^2 \tag{8}$$

In analogy to the FT of the signal, the PSD provides information about the energy distribution, i.e. how much energy is contained in a distinct frequency range. In contrast to the FT amplitude, which is given in the same unit as $x(t)$, the power spectral density has therefore a unit of $\hat{x}^2/\mathrm{Hz}$. As above, PSD can be defined for discrete time series

$$S_{xx}(f) = \lim_{N\to\infty} \frac{(\Delta t)^2}{T} \left| \sum_{n=-N}^{N} x_n e^{-i2\pi fn\Delta t} \right|^2 \tag{9}$$

with the measurement period

$$T = (2N+1)\Delta t \tag{10}$$

going to infinity.

From Eq. 7 and Parseval's theorem Eq. 6 the relation between the total power and the root mean square value (RMS) of the original signal is found to be

$$P = Var(x) = \int_{-\infty}^{\infty} S_{xx}(f) df = RMS^2 \tag{11}$$

This relation allows to calculate an RMS with the same unit as the original signal based on PSD method [9, 10, 11].

This value can be compared to the RMS value of the raw signal:

$$RMS = \sqrt{\frac{1}{N}\left(x_1^2 + x_2^2 + \cdots + x_N^2\right)} \tag{12}$$

For pure sinusoidal signals, the ratio between the RMS amplitude and the actual amplitude of the signal is $1/\sqrt{2}$.

In practice the analysed measurement period T is always finite. Even for a perfectly periodic function $\cos(2\pi ft)$ this leads to spectra with non-zero values at frequencies other than $2\pi f = \omega$, which is called spectral leakage. To reduce this effect a window function can be applied to the signal before FT or PSD are calculated. Commonly used window functions are 1 in the center of the time period of interest and decay towards the borders. Within this study the hamming window

$$w[n] = 0.54 - 0.46 \cdot \cos\left(\frac{2\pi n}{N}\right), \quad 0 \le n \le N \tag{13}$$

is used, here given in a discrete formulation as only discrete signals will be analyzed in this work.

Window functions are also used to divide the whole measurement signal into multiple segments, which can be analyzed individually. This allows to study the frequency content

of a signal over time and is thus more suitable for processes with non-stationary frequencies. One main characteristic of short-time FT (ST-FT and ST-PSD respectively) is that this methodology is constrained by the uncertainty principle, stating that time and frequency resolution can not be narrow at the same time. This relation manifests in the equations used to calculate the window size Δt (in seconds) for spectral analysis for a chosen bin width Δf depending on the underlying sampling frequency f_s

$$N = \frac{f_s}{\Delta f} \rightarrow \Delta t = N \cdot f_s = \frac{1}{\Delta f} \tag{14}$$

If a short time window is used, the resulting bin width Δf is large and thus, the frequency resolution f_{res} of the corresponding spectrum is low [12, 13].

PROBLEM STATEMENT

For ST-FFT calculation window length is a parameter, which is utilized to divide the signal into equal segments before transformation. For longer windows, stochastic or systematic variation of harmonic signal content leads to a reduction of spectral amplitudes. This is illustrated in Fig. 4, which presents the amplitude of the first eigenmode as a function of time for a measurement at design speed. To remove temporal noise, a sliding median of 5 rotor revolutions was applied. During the presented measurement the rotor was throttled continuously until the onset of rotating stall, marked as time 0 in the figure and clearly visible due to immediately rising vibration amplitudes. Two different window sizes, $\Delta t_1 = 0.0312\,\mathrm{s}$ and $\Delta t_2 = 0.0625\,\mathrm{s}$ are compared, which correspond, according to Eq. 14, to a bin width of 32 and 16 Hz respectively. For the lower Δf, the Fourier transformed signal of each 0.031 s period presents a significantly lower amplitude at the frequency of the investigated blade eigenmode. Peak values of the signal with 32 Hz resolution reach 260 μm/m (micro-strain), those of the 16 Hz signal merely 180 before the onset of rotating stall at $t = 0\,\mathrm{s}$. A comparable ratio applies to the average value. This discrepancy is caused by vibration signals with varying frequencies and amplitudes resulting from unsteady forcing during the presented throttling maneuver.

It is obviously a severe problem, as the high-cycle-fatigue limits for the composite material are of the same order of magnitude. Until today, experimental surveillance relies on industrial best-practices, including window size of the ST-FFT. However, the sensitivity must be clearly understood to ensure transferability to scaled geometries, novel architectures, etc..

In order to analyze the influence of the window size on spectral amplitude prediction for more stable operating conditions, Fig. 5 shows the peak-spectrum for the measurement at the last stable operating point ($\mathrm{OP_{DS4}}$) of the design speedline, i.e. the maximum amplitude for each frequency in a total measurement time of 42 s, separated into different window lengths. As above, a strong dependency of spectral amplitude on chosen window length can be recognized for the whole frequency range. Even at stable operating conditions, eigenmode vibration is highly unsteady, resulting in temporally fluctuating vibration frequencies and amplitudes and thus, preventing accurate calculation of spectral amplitudes.

For a small bin width of 4 Hz (i.e. a high frequency resolution) multiple small peaks at integer engine order frequencies are visible besides the dominant eigenmode frequencies of mode 1 and mode 3. These result from synchronous forcing as discussed in [14]. In contrast to Fig. 5, the spectra presented in [14] show averaged spectra of the whole measurement time. While averaging the spectral content has no significant influence on the amplitude of synchronous peaks, as they are only slightly varying in time, the impact on non-synchronous vibration amplitudes is high due to strong time variation. Hence, amplitude of non-synchronous peaks is reduced through averaging, yielding spectra with more distinguished integer EO peaks compared to [14].
Additionally, a second broad 'peak' on the left-hand side of mode 1 can be observed in the 4 and 16 Hz bin width spectra, which can be explained by off-resonant excitation of mode 1 caused by inlet distortions (see [14]). The presence of disturbances near the actual eigenmodes indicates the necessity of high frequency resolutions for proper physical interpretation.

In contrast to the 4 and 16 Hz bin width, the bin width of 96 Hz provides only a coarse approximation of the spectrum. Amplitudes of narrowly spaced peaks are smudged and frequencies corresponding to maximum eigenmode amplitudes are shifted compared to the value obtained by high frequency resolution (i.e. low values of bin width Δf). So far, the real maximum amplitude is unknown, but, as will be shown later, spectral amplitude converges towards the real maximum amplitude for large bin widths.

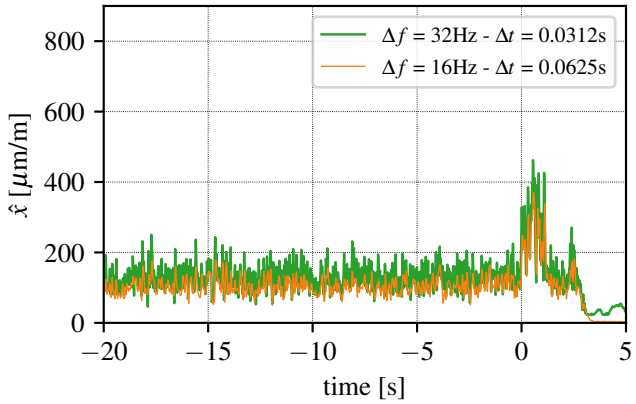

Fig. 4: AMPLITUDE OF FIRST EIGENMODE OVER TIME BEFORE ONSET OF ROTATING STALL FOR DIFFERENT BIN WIDTHS ΔF

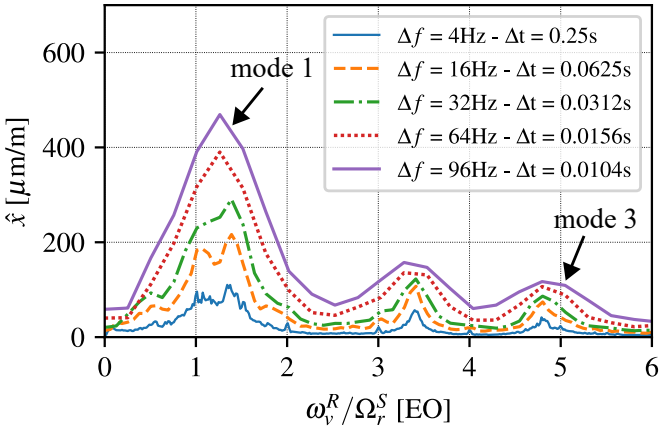

Fig. 5: FFT SPECTRA OF BLADE-MOUNTED STRAIN GAUGE FOR DIFFERENT BIN WIDTHS Δf

Obviously, it is not possible to determine a general window size, which allows for clear identification of phenomena and correct vibration amplitude at the same time.

To quantify the influence of frequency resolution on spectral amplitude, Fig. 6 shows the evolution of the normalized peak amplitude for different modes and operating conditions (mode 1 and mode 3 at OP_{DS4} and mode 1 at OP_{PS4}). In this figure, the bin width, ranging from 1 to 96 Hz, has been normalized with the eigenfrequency f_{mode1} of mode 1. The maximum peak amplitude has been normalized with the respective maximum value of all spectra, which is 472 micro-strain for mode 1 at design speed (corresponding to a bin width of 96 Hz), 118 micro-strain for mode 3 at design speed (corresponding to a bin width of 90 Hz) and 140 micro-strain for mode 1 at part speed (corresponding to a bin width of 96 Hz) respectively.

In Fig. 6 a continuous evolution is visible, showing that for low bin widths the spectral amplitude drops significantly, but in a comparable way for all modes and operating conditions. For higher Δf values, spectral amplitudes show asymptotic behavior.
These results indicate, that an amplitude correction is possible as a function of window size and the respective eigenmode, to combine the possibility of phenomenological interpretation (low bin width) with an accurate value of vibration amplitudes to avoid exceeding scope limits.

The results presented so far do not provide the information, if the asymptotic value corresponds to the real amplitude of the respective mode. This will be discussed in detail in section *Analysis of artificial signals*.

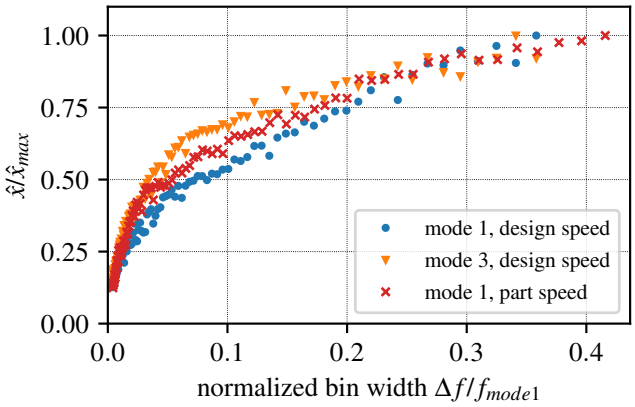

Fig. 6: **MAXIMUM FFT AMPLITUDE AS A FUNCTION OF BIN WIDTH** Δf

Literature proposes to use PSD instead of FFT to avoid influence of chosen window size. For the same measurement signal as before (i.e. operating point OP_{DS4}), Fig. 7 presents PSD spectra, which are obtained with the same window sizes as used in Fig. 5. It is evident that PSD power densities are less dependent from chosen window size compared to FFT amplitudes. However, power density still changes with frequency resolution of up to 40% within the analyzed bin width range. According to Fig. 5, phenomenological interpretation of calculated PSD spectra is difficult for large bin widths due to peak smudging. In addition, PSD power density is given in

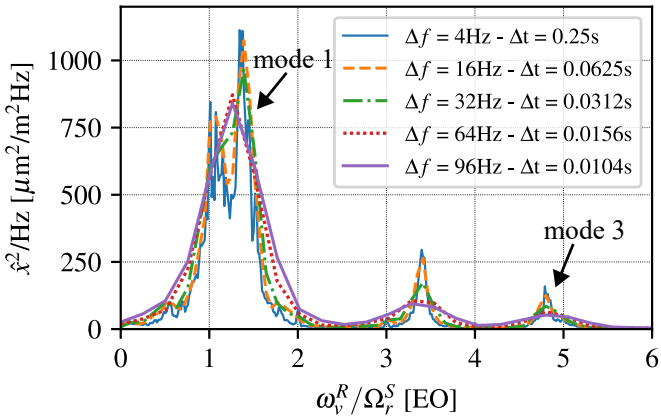

Fig. 7: **PSD SPECTRUM FOR DIFFERENT BIN WIDTHS** Δf

μm^2/m^{2}Hz and thus, not directly comparable to modal scope limits, which are given in $\mu m/m$.
According to Eq. 11, RMS values in micro-strain can be obtained from PSD power densities (in micro-strain^2/Hz) by integrating power spectral density S_{xx} over the frequency range and taking the square root of the result. In the discrete case this is done by multiplying each spectrum in Fig. 7 with the corresponding frequency bin width Δf to receive the RMS value for each frequency f. To allow a better comparison with the FFT spectra shown in Fig. 5, calculated RMS values are multiplied by a factor $\sqrt{2}$ to obtain an approximation of peak amplitudes of harmonic oscillations

$$\hat{x}_{PSD} = \sqrt{2} \cdot RMS = \sqrt{2} \cdot \sqrt{S_{xx,\Delta f} \cdot \Delta f} \tag{15}$$

Fig. 8 shows PSD amplitude $\hat{x}_{PSD}$ (in micro-strain) for the same bin widths as before. It provides the same dependence

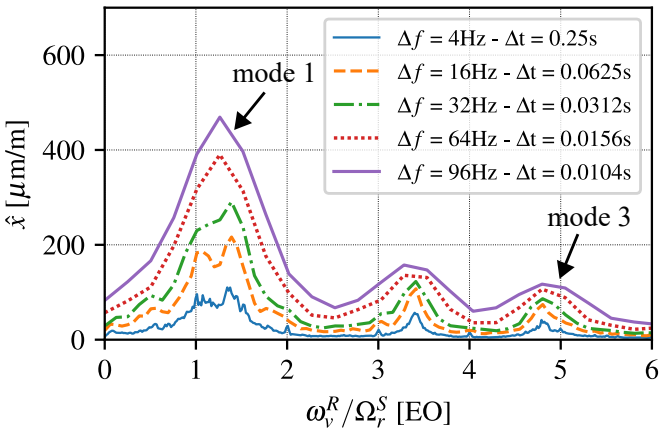

Fig. 8: **RMS SPECTRA BASED ON PSD CALCULATION FOR DIFFERENT BIN WIDTHS** Δf

of spectral amplitude on bin width but amplitudes are in good agreement with Fig. 5 for all bin widths.

Hence, peak spectra calculation based on PSD is not beneficial for vibration monitoring, if comparison with material- and eigenmode-dependent scope limits are required.

ANALYSIS OF ARTIFICIAL SIGNALS

Fig. 6 shows spectral peak amplitudes, which reach an asymptotic value for low frequency resolution i.e. high values of Δf. As stated in the previous section, it is not clear,

if the asymptotic value corresponds to the real maximum amplitude of the respective eigenmode. To allow for systematic parameter analysis, artificial signals with known amplitudes are studied in the following.

Mass-oscillator model

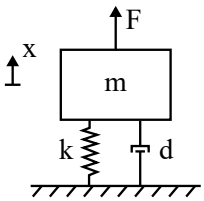

Fig. 9: **SDOF MASS OSCILLATOR**

To approximate the vibratory behavior of the rotor blades, a forced single degree of freedom (SDOF) mass oscillator according to Fig. 9 was simulated, which follows the differential equation

$$m\ddot{x} + d\dot{x} + kx = F \tag{16}$$

Using

$$\frac{d}{m} = 2\zeta\omega_0 \quad \text{and} \quad \frac{k}{m} = \omega_0^2 \tag{17}$$

to substitute stiffness k and viscous damping ratio d, Eq. 16 can be expressed by means of natural frequency ω_0 and damping ratio ζ [15]

$$\ddot{x} + 2\zeta\omega_0\dot{x} + \omega_0^2 x = \frac{F}{m} \tag{18}$$

Excitation of the system was applied through the force F

$$F = \hat{f}_1(t)\cos\left(\omega_{f1}(t)t\right) + \hat{f}_2(t)\cos\left(\omega_{f2}(t)t\right) \tag{19}$$

with stochastically varying amplitude $\hat{f}$. Excitation frequency ω_f was chosen to vary in time with a frequency of $\omega_{f,dist}$ and a stochastically varying amplitude of $\hat{x}_{dist}$ around the mean value ω_{f0}

$$\begin{aligned} \omega_{f1}(t) &= \omega_{f0} + \hat{x}_{dist,1} \\ \omega_{f2}(t) &= \omega_{f0} + \hat{x}_{dist,2}\cos\left(\omega_{f,dist}t\right) \end{aligned} \tag{20}$$

Table 1 summarizes the parameters used to simulate the SDOF mass oscillator motion. Parameters have been adjusted to achieve signals with comparable spectral content to those observed in the aeroelastic measurements.
The mean forcing frequency was chosen to be equal to the eigenfrequency of the system $\omega_{f0} = \omega_0$. For the first part of the excitation f_1 this mean frequency varies randomly with an amplitude of $\hat{x}_{dist1} = 1\,\text{Hz}$, i.e. less than 0.5% of the eigenfrequency. In the second part of the excitation f_2, the forcing amplitude $\hat{f}_2$ is higher compared to $\hat{f}_1$, but variation of forcing frequency is increased at the same time, resulting in a broad excitation of multiple frequencies. The amplitude of forcing frequency variation ω_{f2} was chosen to vary harmonically with 12 Hz and in addition stochastically with 3 Hz, yielding an overall amplitude of $\hat{x}_{dist2} = 15\,\text{Hz}$, which corresponds to 6% ω_0.

Table 1: **PARAMETER FOR THE SDOF MASS OSCILLATOR MODEL**

eigenfrequency ω_0	$2\pi \cdot 250\,\text{Hz}$
damping ratio ζ	0.02
mean forcing frequency ω_{f0}	$2\pi \cdot 250\,\text{Hz}$
frequency of forcing disturbance $\omega_{f,dist}$	$2\pi \cdot 3.5\,\text{Hz}$
amplitude of forcing disturbance $\hat{x}_{dist,1}$	$2\pi \cdot 1\,\text{Hz}$
$\hat{x}_{dist,2}$	$2\pi \cdot 15\,\text{Hz}$

Influence of bin width

Integrating Eq. 18 yields the displacement $x(t)$ of the mass m (see Fig. 10), which can be treated in the same way as the signals of rotor strain gauges in the previous section.

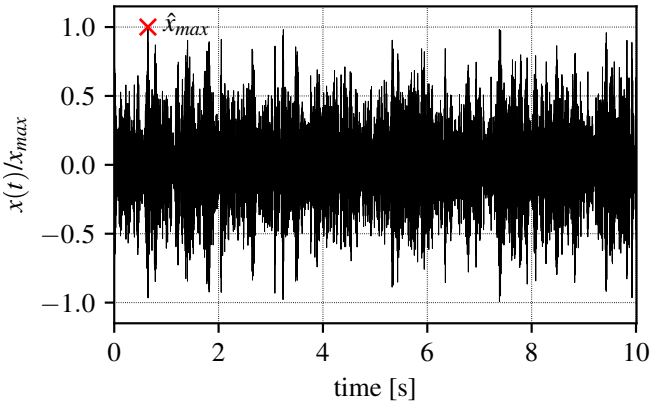

Fig. 10: **DISPLACEMENT SIGNAL** $x(t)$ **OF SDOF MASS OSCILLATOR,** $\zeta = 0.02$

Fig. 11a) and Fig. 11b) show spectra (maximum amplitude during a simulation time of $t_{SDOF} = 10\,\text{s}$) of the signal $x(t)$ for different bin widths calculated using FFT and PSD method respectively. FFT spectra have been normalized with the maximum amplitude as indicated by the red cross in Fig. 10 and PSD spectra with the maximum power spectral density of the 4 Hz bin width spectrum.
In accordance to Fig. 5 and Fig. 7, Fig. 11 shows a dependence of calculated FFT and PSD amplitude on chosen bin width. A decreased window size leads to increased spectral amplitudes, if FFT method is used, whereas this behavior is reversed for PSD application. Fig. 11a) proves that spectral amplitudes predicted with short windows i.e. large bin widths are close to the real maximum amplitude, while they are more than 50% to low, if a bin width of 4 Hz is used. In contrast to that, PSD amplitude is reduced up to 80% for large bin widths compared to the value for $\Delta f = 4\,\text{Hz}$.

To study this relation of the FFT amplitude in more detail, Fig. 12 shows the peak spectral amplitude of the SDOF

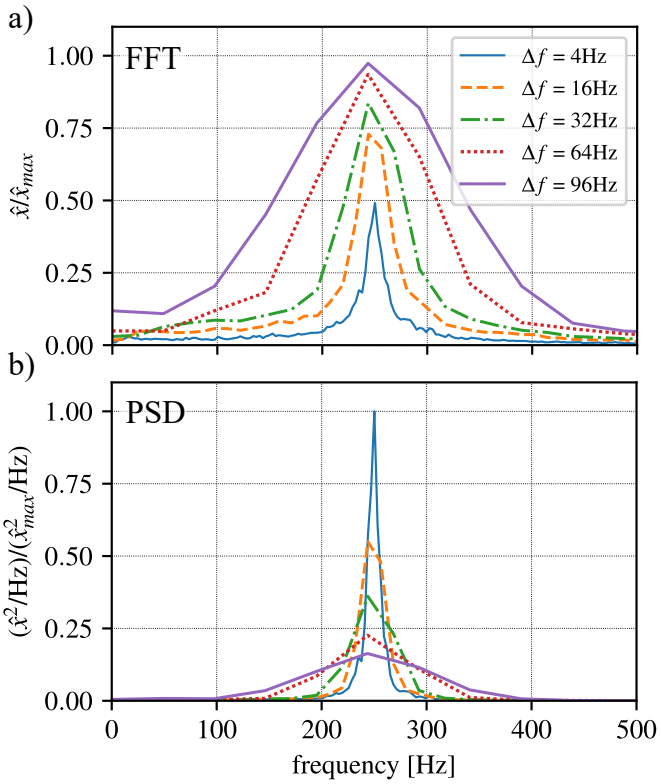

Fig. 11: **SPECTRA OF DISPLACEMENT SIGNAL $x(t)$ OF SDOF MASS OSCILLATOR FOR DIFFERENT BIN WIDTHS Δf: a) FFT, b) PSD**

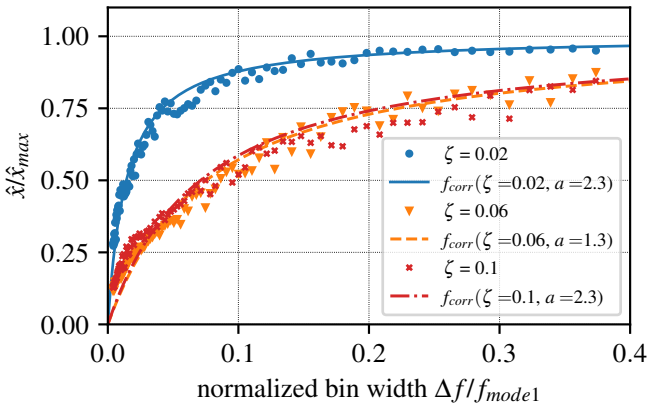

Fig. 12: **MAXIMUM FFT AMPLITUDE OF SDOF MASS OSCILLATOR FOR DIFFERENT BIN WIDTHS Δf AND DAMPING RATIOS ζ**

model with $\zeta = 0.02$ (blue dots) as a function of normalized bin width similar to Fig. 6. In this figure, spectral amplitude has been normalized with the real maximum amplitude of the signal $x(t)$ during the total simulation time of 10 s (red cross in Fig. 10). This normalization provides a good agreement of spectral amplitudes calculated with high Δf values and the real amplitude of the SDOF mass oscillator with low damping ratio, indicated by an asymptotic value of 1. This observation proves that it is possible to obtain the correct amplitude of vibratory signals, if large bin widths i.e. small time windows resulting in a low frequency resolution, are utilized. In the case of the artificial signal, the disturbance frequency is with about 6% ω_0 low, resulting in a relatively harmonic signal. Compared to Fig. 6 the asymptotic value is reached at a smaller normalized bin width $\Delta f \approx 0.2$, indicating that damping or broadband forcing are higher in the experiment.

Influence of modal damping

If the damping ratio is increased, the slope of the curve in the small bin width region is reduced and calculated spectral amplitude is more sensitive to bin width variation. The highest value for $\zeta = 0.06$ and $\zeta = 0.1$ is around 90% $\hat{x}_{max}$, hence the error between real and estimated maximum amplitude is larger compared to the low-damped case. This is the result of a signal $x(t)$, which is closer to a pure harmonic oscillation for lower damping ratios. Obviously, FFT application works better in this case and calculated spectral amplitude is closer to the real maximum amplitude for all bin widths.

For damping ratios higher than $\zeta = 0.05$ the influence of the bin width is not further increased, yielding nearly identical relations between normalized bin width and spectral amplitude for $\zeta = 0.06$ and $\zeta = 0.1$ in Fig. 12.

The comparison of Fig. 6 and Fig. 12 indicates that the different curve forms for the cases shown in Fig. 6 are related to different damping ratios. It remains hence inevitable to integrate damping of specific modes for spectral amplitude correction.

For turbomachinery blades mainly three mechanisms contribute to overall damping of the system: material (within blades), mechanical (blade/disc contact etc.) and aerodynamic damping. For the analyzed UHBR fan architecture, material and mechanical damping are low compared to aerodynamic damping (order 0.2%). Remaining aerodynamic damping depends on operating conditions i.e. massflow and pressure ratio as well as on the analyzed eigenmode. Numerical simulations indicate an order of a few percent aerodynamic damping as long as no aeroelastic instability mechanism such as flutter or NSV [16] is present.

If the vibratory response of a system to an excitation $F(\omega)$ in the frequency domain i.e. the FFT amplitude spectrum is known, eigenfrequency ω_0, stiffness k and damping ratio ζ can be determined using the transfer function

$$H(\omega) = \frac{X(\omega)}{F(\omega)} \tag{21}$$

For the SDOF mass oscillator the magnitude of the transfer function is given by

$$|H(\omega)| = \frac{1}{k^*} \frac{1}{\sqrt{\left(1 - \frac{\omega^2}{\omega_0^2}\right)^2 + \left(2\zeta\frac{\omega}{\omega_0}\right)^2}} \tag{22}$$

where k^* is the normalized stiffness k/f_0 of the system [15]. Eq. 22 is utilized in a least square curve fit algorithm and applied to FFT spectra with different bin widths. For the SDOF model good agreement between pre-selected damping ratio ζ and the value estimated by the curve fit algorithm is achieved, if the spectrum corresponding to very small bin widths, for example $\Delta f = 1$ Hz is considered as system response. These small bin widths result in spectra with a very high frequency resolution, thus allowing a very easy differentiation of peaks caused by engine order, off-resonant and resonant excitation. Hence, application of the curve fit algorithm to these spectra enables accurate determination of eigenfrequency and damp-

ing ratio. In the spectra presented above, the bin width of $\Delta f = 1\,\mathrm{Hz}$ is not shown, as it is not suitable for vibration monitoring due to the large window size of $\Delta t = 1\,\mathrm{s}$.

To determine (aerodynamic) damping for the measurement signals shown in Fig. 6, the curve fit method was applied to FFT spectra (with a bin width of 1 Hz) of the respective strain gauge data. Fig. 13 presents an example of fitted curves for the last stable operating point $\mathrm{OP}_{\mathrm{DS4}}$ of the design speed measurement and corresponding estimated damping ratios are indicated in the legend.

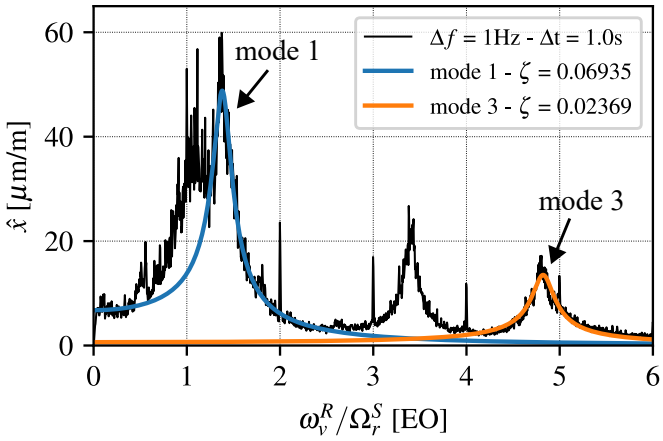

Fig. 13: **RESULT OF CURVE FIT METHOD FOR STRAIN GAUGE MEASUREMENT DATA AT DESIGN SPEED**

Comparison of Fig.6 and Fig. 12 together with the values for the damping ratio ζ obtained by the curve fit procedure Fig. 13 explains the difference between mode 1 and mode 3 in Fig. 6. The damping ratio of mode 3 is about 3.2 times lower than the damping ratio of mode 1 and thus spectral amplitude is less sensitive to bin width variation, especially for normalized bin widths $0.04 \leq \Delta f / f_{mode1} \leq 0.2$.

For mode 1 of the part speed measurement shown in Fig. 6 damping ratio was found to be around $\zeta = 0.08$ and thus higher than for mode 1 at design speed. Above, it was stated that the influence of damping is not further increased for damping ratios higher than 0.05 and curves for higher damping ratios should be nearly identical. Hence, mode 1 curves in Fig. 6 should be closer to each other due to high damping ratios.

During adjustment of the parameters of the SDOF model (summarized in Table 1) it was observed that changing the forcing amplitude ($\hat{f}_1$ and $\hat{f}_2$ and frequency variation ($\omega_{f,dist}$, $\hat{x}_{dist,1}$ and $\hat{x}_{dist,2}$) has an impact on the relation of spectral amplitude and bin width even if this influence is lower compared to that of the damping ratio ζ. The difference for mode 1 visible in Fig. 6 between part and design speed might therefore occur due to different forcing mechanisms.

CORRECTION APPROACH

In the previous sections it has been shown that the spectral amplitude estimation strongly depends on chosen window size. The specific relation between both quantities is influenced by multiple parameters such as operating conditions and investigated eigenmode. However, the trend (strong drop of amplitude for small and asymptotic behavior for large bin widths) is similar for all investigated cases, indicating that correction of spectral amplitude depending on chosen window size might be a promising concept for dealing with this dependency.

Using the SDOF model, it was possible to determine damping ratio ζ as a parameter with a major impact on the relation between frequency resolution and spectral amplitude. In this section, this information is used to develop a function, which approximates the behavior shown in Fig. 6 depending on the corresponding damping ratio for each case.

The function used for approximation is given by

$$f_{corr}(a) = \frac{1}{e^1 - 1}\left(e^{1-\frac{1}{\frac{a}{\zeta}\Delta f^* + 1}} - 1\right)$$
$$\Delta f^* = \frac{\Delta f}{f_{mode1}} \tag{23}$$

with the damping ratio ζ and the correction parameter a. The latter is used to fit Eq. 23 to the data sets presented in Fig. 6 and Fig. 12 and thus, accounting for other influencing parameter such as forcing mechanism. Eq. 23 provides a drop in amplitude for small bin widths and an asymptotic value of 1 is reached for $\Delta f \to \infty$. Fig. 12 illustrates the correction function f_{corr} for the same damping ratios used to simulate the SDOF mass oscillator. It provides good agreement between model and correction function for fitting parameter $a = 2.3, 1.3$ and 2.3 respectively.

In the previous section it was observed, that increasing ζ beyond a specific value of $\zeta \approx 0.05$ does not further reduce the predicted spectral amplitude. Hence, the correction parameter a will increase for values $\zeta = 0.05$ to prevent approximation curves from becoming to flat.

The approximation shown in Fig. 12 is used to correct spectral amplitudes for a given bin width Δf according to

$$\hat{x}_{corr}(\Delta f^*) = \frac{1}{f_{corr}(\Delta f^*)} \cdot \hat{x}(\Delta f^*) \tag{24}$$

for the eigenmodes under investigation.

As damping can only be determined for eigenmodes, i.e. distinct frequencies in the continuous spectrum, correction function Eq.23 (correction parameter a and damping ratio ζ) can be interpolated for all other frequencies between f_{mode1} and f_{mode3}, if visualization of continuous corrected spectra is desired.

RESULTS AND DISCUSSION

Application of the correction with the damping ratios from Fig. 13 and correction parameters a derived by fitting Eq. 23 to the cases presented in Fig. 6 delivers the graphs in Fig. 14. For mode 1 consistent peak amplitude of approximately 520 micro-strain is derived for all Δf larger than 4 Hz. Mode 3 amplitude is estimated to approximately 120 micro-strain.

The real maximum amplitude, necessary to evaluate soectral amplitudes of different bin widths, is estimated using the maximum spectral amplitude **without** correction $\hat{x}_{FFT,max}$ (represented by a value of 1 in Fig. 6 due to normalization and corresponding to high bin widths between 90 and 96 Hz). According to Fig. 12, the maximum spectral amplitude of

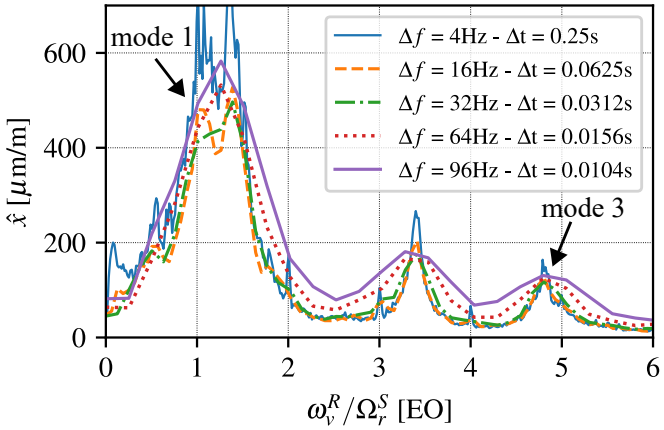

Fig. 14: **CORRECTED FFT SPECTRA OF BLADE-MOUNTED STRAIN GAUGE FOR DIFFERENT BIN WIDTHS Δf**

the SDOF model corresponds to $b = 90\%$ to 95% of the real maximum amplitude of the mass oscillator for $\zeta = 0.02$ and $\zeta = 0.05 - 0.1$ respectively. This information allows to approximate the real maximum amplitude using

$$\hat{x}_{max} = b \cdot \hat{x}_{FFT,max} \tag{25}$$

Eq. 25 yields a maximum amplitude for mode 1 of 472 micro-strain $\cdot 1.11 = 520$ micro-strain and for mode 3 118 micro-strain $\cdot 1.05 = 124$ micro-strain, which is in good agreement with Fig. 14 except for the smallest bin width. For $\Delta f = 4\,\mathrm{Hz}$ the amplitude is over-predicted after the correction, especially for mode 1.

The evolution over bin width is visualized in Fig. 15, normalized with the estimated maximum amplitude. It can be seen that for frequency bin widths larger than 5% of the modal frequency f_{mode1}, i.e. $\Delta f \approx 14\,\mathrm{Hz}$, the corrected amplitude is robustly estimated within a range of $\pm 8\%$ for all investigated modes and operating points.

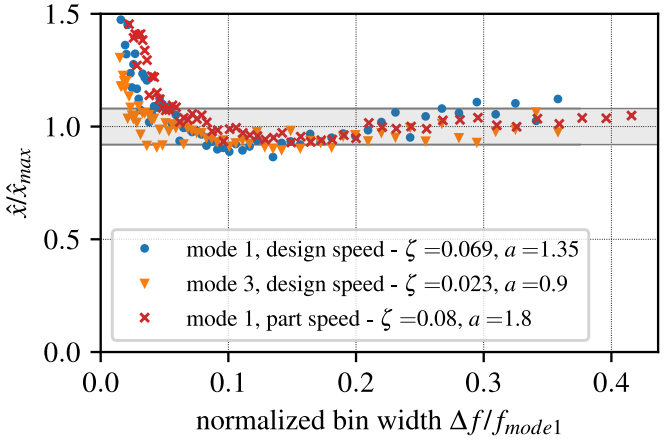

Fig. 15: **CORRECTED MAXIMUM FFT AMPLITUDE AS A FUNCTION OF BIN WIDTH Δf**

The visualization provides a good agreement of calculated spectral amplitude and (estimated) real maximum amplitude, resulting in values close to 1. Only in the small bin width region (i.e. for high frequency resolutions) the amplitude is over-corrected in all cases. The error after correction leads to a conservative amplitude prediction, which is much less dangerous during machine operation. In a wide range between normalized bin widths of $0.06 \leq \Delta f \leq 0.4$, the corrected spectral amplitude is mostly independent of the resolution. This allows to derive a clear guideline for correcting spectral amplitude depending on desired frequency resolution and analyzed eigenmode. Based on known eigenfrequencies, a reasonably small frequency bin width ($\Delta f \geq 5\%\ f_{mode1} \approx 14\,\mathrm{Hz}$) can be selected, and a correction function derived.
The whole procedure can be summarized as follows:

1. Perform initial measurement at stable operating conditions
2. Determine modal damping for each mode based on a FFT spectra and the transfer function Eq.22
3. Validate amplitude evolution with different bin widths in post-processing and perform curve fit of Eq. 23 to derive correction parameter a
4. Use damping ratio ζ and correction parameter a to correct spectral amplitude depending on desired bin width and investigated eigenmode

If desired, determined correction parameter ζ and a can be interpolated for frequency range dependent correction of continuous spectra.

This correction approach allows for a robust use of window sizes for ST-FFT in a range, which is suitable for online turbomachinery surveillance, but very sensitive due to the sharp slope in Fig.6 (between 0.05 and 0.1) and the absolute value which is underestimated by the order of 30-50% if uncorrected.

Exemplarily, the correction approach has been applied to the time-resolved amplitude of the first eigenmode during throttling of the rotor as shown in Fig. 4.

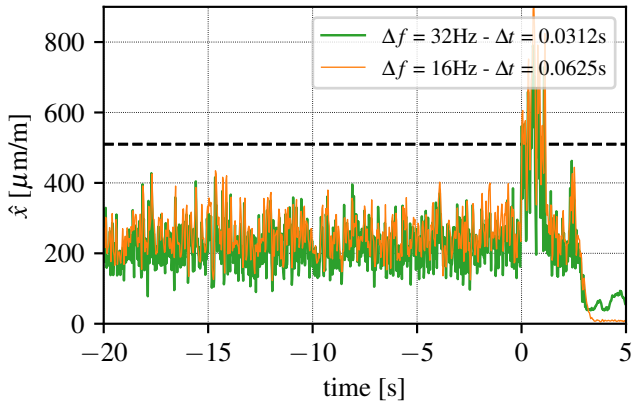

Fig. 16: **CORRECTED AMPLITUDE OF FIRST EIGENMODE OVER TIME FOR DIFFERENT BIN WIDTHS Δf**

The real maximum amplitude within the 20 s before stall onset, is estimated as above, by calculating a spectrum with a large bin width of 96 Hz and multiplying the maximum spectral amplitude of mode 1 with 1.11, resulting in a value of 510 micro-strain (indicated by the black dashed line in Fig. 16). In contrast to Fig. 5, the curves for both frequency resolutions are at constant level before stall onset ($t = 0\,\mathrm{s}$), reaching peak values of 400 micro-strain. Hence, derived amplitudes are still slightly too low due to application of the sliding median.

After stall onset, HCF limit is surpassed, but now consistently estimated independent of the chosen frequency resolution, i.e. frequency bin width.

Fig. 16 is a strong improvement compared to Fig. 4, thus confirming the applicability of the presented correction approach during machine operation surveillance.

CONCLUSION

Blade vibration monitoring is mandatory during measurements to ensure safe operation of the facility and the structural integrity. During a measurement campaign on the transonic fan test facility a strong dependence of calculated spectral amplitudes (using FFT and PSD methods) on window length has been identified. This is related to vibration signals, which consist of dominant frequency peaks related to eigenmodes, but disturbed by temporal fluctuations caused by different phenomena (forced response, lock-in, etc.). For large window sizes a high frequency resolution (i.e. small bin width) is achieved, but estimated vibrational amplitude of different eigenmodes is up to 90% lower compared to small window sizes. The exact relation between window size and spectral amplitude has shown to be a function of operating conditions and analyzed eigenmode depending on the corresponding damping ratio.

Using a SDOF model it was possible to show that the correct maximum amplitude of the signal is only captured by spectral methods if very short windows are used. Due to the uncertainty principle they result in coarse spectra, which prevent differentiation of narrowly spaced peaks and determination of exact eigenfrequencies.

Therefore, a correction approach has been developed, which corrects calculated spectral amplitudes based on preselected window size and damping ratio. This allows the utilization of longer windows with the benefit of highly resolved spectra and reliable amplitude prediction at the same time, within suitable ranges for transient turbomachinery experiments.

The proposed method allows a more purposeful determination of safety factors, evaluation parameters and a robust implementation.

ACKNOWLEDGMENT

The presented research was supported through the European Union's Seventh Framework Programme for research, technological development and demonstration, ENOVAL, grant agreement N604999 and the Clean Sky 2 Joint Undertaking (JU) under grant agreement N864719, CATANA. The JU receives support from the European Union's Horizon 2020 research and innovation programme and the Clean Sky 2 JU members other than the Union. The paper reflects only the author's view and the JU is not responsible for any use that may be made of the information it contains. Assessment of the test facility was enabled through financial supports of Agence Nationale de la Recherche (ANR, Project d'EqupEx PHARE) and Conseil pour la Recherche Aeronautique Civile (CORAC - Programme CUMIN). Buildings and infrastructure were supported by ECL, instrumentation supported by Institut Carnot (INGENIERIE@LYON - Project MERIT). We are grateful for the continuous collaboration and financial support of SAFRAN AE since the beginning of this project and specifically for the present measurement campaign. The authors would like to particularly acknowledge the precious contributions of Gilbert Halter, Lionel Pierrard, Pierre Laucher and Sebastien Goguey.

REFERENCES

[1] Brandstetter, C., Pagès, V., Duquesne, P., Ottavy, X., Ferrand, P., Aubert, S., and Blanc, L., 2021. "Uhbr open-test-case fan ecl5/catana part 1: Geometry and aerodynamic performance". In 14th European Conference on Turbomachinery Fluid dynamics & Thermodynamics.

[2] Pagès, V., Duquesne, P., Ottavy, X., Ferrand, P., Aubert, S., Blanc, L., and Brandstetter, C., 2021. "Uhbr open-test-case fan ecl5/catana, part 2: Mechanical and aeroelastic stability analysis". In 14th European Conference on Turbomachinery Fluid dynamics & Thermodynamics.

[3] Russell, J., 1953. "Wake survey and straingauge measurements on an inclined propeller in the rae 24 ft. tunnel. part 1: wake survey".

[4] Drew, D., 1958. "Developments in methods of measuring stresses in compressor and turbine blades on test bed and in flight". *Proceedings of the Institution of Mechanical Engineers, 172*(1), pp. 320–359.

[5] Hohenberg, R., 1967. "Detection and study of compressor-blade vibration". *Experimental Mechanics, 7*(6), pp. 19A–24A.

[6] Brandstetter, C., Ottavy, X., Paoletti, B., and Stapelfeldt, S., 2021. "Interpretation of stall precursor signatures". *Journal of Turbomachinery, 143*(12), p. 121011.

[7] Siemens, 2020. What is a power spectral density (psd)? https://community.sw.siemens.com/s/article/what-is-a-power-spectral-density-psd. Accessed: 2022-07-31.

[8] Brandstetter, C., Duquesne, P., Paoletti, B., Aubert, S., Ottavy, X., and Others, 2019. "Project PHARE-2—A High-Speed UHBR Fan Test Facility for a New Open-Test Case". *Journal of Turbomachinery, 141*(10).

[9] Butz, T., 2015. *Fourier transformation for pedestrians*. Springer.

[10] Stoica, P., Moses, R. L., et al., 2005. *Spectral analysis of signals*, Vol. 452. Pearson Prentice Hall Upper Saddle River, NJ.

[11] Alessio, S. M., 2015. *Digital signal processing and spectral analysis for scientists: concepts and applications*. Springer.

[12] Cohen, L., 1995. *Time-frequency analysis*, Vol. 778. Prentice hall New Jersey.

[13] Neubauer, A., 2012. *DFT-Diskrete Fourier-Transformation: Elementare Einführung*. Springer-Verlag.

[14] Schneider, A. P., Paoletti, B., Ottavy, X., and Brandstetter, C., 2022. "Influence of a turbulence control screen on the aerodynamic and aeroelastic behavior of a UHBR fan".

[15] Mukhopadhyay, M., 2021. *Structural Dynamics: Vibrations and Systems*. Springer Nature.

[16] Stapelfeldt, S., and Brandstetter, C., 2022. "Suppression of nonsynchronous vibration through intentional aerodynamic and structural mistuning". *Journal of Turbomachinery, 144*(2).